Diallyl trisulfide induces apoptosis by suppressing NF-κB signaling through destabilization of TRAF6 in primary effusion lymphoma

ZENPEI SHIGEMI[1], YOSHIKI FURUKAWA[1], KOHEI HOSOKAWA[1], SETSUYA MINAMI[1], JUMPEI MATSUHIRO[1],
SHIORI NAKATA[1], TADASHI WATANABE[1], HIROKI KAGAWA[1], KOJI NAKAGAWA[2],
HIROSHI TAKEDA[2] and MASAHIRO FUJIMURO[1]

[1]Department of Cell Biology, Kyoto Pharmaceutical University, Yamashinaku, Kyoto 607-8412;
[2]Department of Pathophysiology and Therapeutics, Faculty of Pharmaceutical Sciences,
Hokkaido University, Kitaku, Sapporo 060-0812, Japan

Abstract. The allyl sulfides, including diallyl sulfide (DAS), diallyl disulfide (DAD), and diallyl trisulfide (DAT), contained in garlic and members of the Allium family, have a variety of pharmacological activities. Therefore, allyl sulfides have been evaluated as potential novel chemotherapeutic agents. Here, we found that DAT inhibited nuclear factor-κB (NF-κB) signaling and induced apoptosis in primary effusion lymphoma (PEL), a subtype of non-Hodgkin's B-cell lymphoma caused by Kaposi's sarcoma-associated herpesvirus (KSHV). We examined the cytotoxic effects of DAS, DAD and DAT on PEL cells. DAT significantly reduced the viability of PEL cells compared with uninfected B-lymphoma cells, and induced the apoptosis of PEL cells by activating caspase-9. DAT induced stabilization of IκBα, and suppressed NF-κB transcriptional activity in PEL cells. We examined the mechanism underlying DAT-mediated IκBα stabilization. The results indicated that DAT stabilized IκBα by inhibiting the phosphorylation of IκBα by the IκB kinase (IKK) complex. Furthermore, DAT induced proteasomal degradation of TRAF6, and DAT suppressed IKKβ-phosphorylation through downregulation of TRAF6. It is known that activation of NF-κB is essential for survival of PEL cells. In fact, the NF-κB inhibitor BAY11-7082 induced apoptosis in PEL cells. In addition, DAT suppressed the production of progeny virus from PEL cells. The administration of DAT suppressed the development of PEL cells and ascites in SCID mice xenografted with PEL cells. These findings provide evidence that DAT has antitumor activity against PEL cells *in vitro* and *in vivo*, suggesting it to be a novel therapeutic agent for the treatment of PEL.

Introduction

Primary effusion lymphoma (PEL, also termed body-cavity-based lymphoma) is a malignant B-cell lymphoma caused by Kaposi's sarcoma-associated herpesvirus (KSHV, also named HHV-8) in immunosuppressed individuals, such as AIDS patients or those that have undergone organ transplantation (1,2). PEL is a subtype of non-Hodgkin's lymphoma and is characterized by lymphomatous effusions of pleural and abdominal cavities. KSHV is a rhadinovirus of the γ-herpesvirus subfamily and is closely related to herpesvirus Saimiri and Epstein-Barr virus (EBV). KSHV is the causative agent of Kaposi's sarcoma and AIDS-related lymphoproliferative disorders, such as PEL and multicentric Castleman's disease (3). Similar to other herpesviruses, KSHV has two life cycles (latency and lytic replication). The KSHV genome circularizes and forms a double-stranded DNA, the episome, in the nucleus of PEL cells during latent infection. To establish a latent infection, KSHV expresses several viral genes, including latency-associated nuclear antigen (LANA), v-FLIP, v-cyclin, kaposin and microRNAs, in PEL cells. LANA is required for the replication and maintenance of viral DNA, and contributes to KSHV-associated oncogenesis through interaction with cellular molecules, such as p53, Rb and GSK-3. These viral proteins and RNA manipulate cellular signaling pathways, including nuclear factor-κB (NF-κB), Akt, Wnt and Erk, to maintain the malignant phenotype and ensure PEL cell survival (4-6). Especially, NF-κB signaling is constitutively activated in KSHV-infected PEL cells to facilitate anti-apoptosis and growth (7-11). KSHV alternates between lytic replication and latency by RTA expression. RTA, encoded by the immediate-early gene ORF50, is a critical switch molecule for initiating lytic replication.

In canonical NF-κB signaling, the NF-κB transcription factor, which is a heterodimer of p50 and p65/RelA, is retained in the cytosol by interaction with IκBα (12). IκBα is further regulated by the IκB kinase (IKK) complex, consisting of IKKα, IKKβ and IKKγ/NEMO. A stimulus, such as LPS or IL-1β, induces activation of TRAF6 through MyD88 and IRAK, and TRAF6 induces the activation of TAK1-TAB2 complex, which phosphorylates the catalytic subunit IKKβ and activates the IKK complex (13). TRAF6, an E3 ubiquitin ligase, can modify IKKγ and TRAF6 itself via K63-linked polyubiquitination, and K63-linked polyubiquitination of IKKγ and TRAF6 contributes to the activation of IKK complex (14). The activated IKK complex phosphorylates Ser32 and Ser36 of IκBα. Phosphorylated IκBα is polyubiquitinated by ubiquitin ligase E3 and subsequently destabilized by proteasomal degradation. This degradation of IκBα leads to nuclear translocation of NF-κB and the NF-κB-dependent transcriptional activation.

Garlic (*Allium sativum* L.) is widely used in traditional herbal remedies and alternative medicine. Garlic oil from fresh garlic contains allyl sulfides, including diallyl sulfide (DAS), diallyl disulfide (DAD), diallyl trisulfide (DAT), and other allyl polysulfides (15). The proportions of allyl sulfides in garlic oil are ~6% DAS, 30% DAD, 40% DAT and 24% other analogs (16). Allyl sulfides have many biological functions, including suppression of inflammation, upregulation of detoxification, enhancement of histone acetylation, generation (or reduction) of reactive oxygen species (ROS), and induction of endoplasmic reticulum (ER) stress (17,18). There have been many reports of anticancer effects of these compounds against a variety of cancers, including prostate, lung, breast, and colon cancer cells (19-22). In addition, DAT directly produces ROS through the homolytic cleavage of intramolecular trisulfide bonds, and DAT-mediated ROS induces oxidative and ER stress, causing apoptosis of various cancer cell types (20-23). Recently, DAT has been shown to affect cellular signaling pathways including Akt, NF-κB, Jnk and Erk, in tumor cells (24,25).

PEL is an aggressive lymphoma caused by KSHV, and is resistant to chemotherapy regimens, such as CHOP and R-CHOP (26). Therefore, the development of novel and effective drugs for PEL is required. Regarding biological properties of allyl sulfides, these could be novel compounds used with molecular target drugs for the treatment of PEL. The anticancer effect of allyl sulfides against PEL remains unknown; we therefore investigated whether allyl sulfides kill PEL cells and the underlying molecular mechanism thereof.

Materials and methods

Cells and reagents. KSHV-positive PEL cell lines (BC2, BC3, BCBL1 and HBL6) and KSHV-negative lymphoma cell lines (Ramos, BJAB and DG75) were maintained in RPMI-1640 medium supplemented with 10% fetal calf serum. DAS (Wako, Osaka, Japan), DAD (Tokyo Chemical Industry, Tokyo, Japan), DAT (LKT Laboratories, St. Paul, MN, USA) were dissolved in dimethyl sulfoxide (DMSO).

Cell viability assay. Cells were seeded on 96-well plates at $2.5x10^4$ cells/well in 100 μl of medium with or without various concentrations of DAS, DAD or DAT and then incubated at

37˚C for 24 h. The number of viable cells was estimated using a Cell Counting kit-8 (Dojindo, Tokyo, Japan) as described previously (27). The optical density at 450 nm of each sample was measured using a microplate spectrophotometer (Tecan M200; Tecan, Kanagawa, Japan) and expressed as a percentage of the value in untreated cells (defined as 100%). Data are shown as the means ± SEM of three independent experiments.

Western blotting and antibodies. Western blotting was performed as described previously (28). Primary antibodies used in these experiments included those against Ser32/36-phospho-IκBα, Ser176/180-phospho-IKKα/β, caspase-3, -7, -8, -9 and PARP (Cell Signaling Technology, Danvers, MA, USA), IκBα, p65, and p21Cip1 (BD Biosciences, Franklin Lakes, NJ, USA), β-actin, histone H2B, K-bZIP and S-tag (Santa Cruz Biotechnology, Inc., Santa Cruz, CA, USA). FK2 that we established previously (29) was used to detect polyubiquitin molecules.

Caspase assay. To measure caspase activity, $1.0x10^5$ BC3 PEL cells/well were added to 1 ml of medium and incubated with DAT for 3 h. Activities of caspase-8 and -9 in cell lysates were measured using a caspase-Glo assay kit (Promega, Madison, WI, USA) with luciferin-conjugated LETD or LEHD polypeptide, respectively, according to the manufacturer's instructions. Luminescence was detected using a GloMax 20/20 luminometer (Promega). The caspase activity in untreated cells was defined as 1.0 relative light unit.

Immunofluorescence (IF) analysis. Prior to IF analysis, BCBL1 cells were treated with 10 μM DAT for 18 h and fixed in methanol on glass slides followed by incubation with primary antibodies for 1 h. After washing, the cells were incubated with Alexa Fluor 594-conjugated donkey anti-mouse IgG or Alexa Fluor 488-conjugated donkey anti-rabbit IgG (Invitrogen, Carlsbad, CA, USA). To stain the nuclei, cells were incubated in 4 ng/ml of DAPI in PBS during binding of the secondary antibody. Immunofluorescence images were obtained by fluorescence microscopy (IX71; Olympus, Tokyo, Japan).

Nuclear protein extraction. Harvested cells were incubated with hypotonic buffer containing 10 mM HEPES (pH 7.9), 10 mM KCl, 0.1 mM EDTA, 0.1 mM EGTA, 0.1 mM PMSF, and 1 mM DTT on ice for 15 min, and then cells were lysed by addition of NP-40 (final concentration, 0.6%) and heavy agitation with a vortex mixer. Cell lysates were centrifuged at 15,000 rpm for 30 sec at 4˚C. The nuclear pellets were rinsed with the hypotonic buffer supplemented with 0.6% NP-40. The obtained nuclear extracts were lysed in SDS-PAGE sample buffer.

Luciferase reporter assay. BC3 cells ($1x10^5$) were transfected with 2 μg of NF-κB-luciferase reporter (pGL4.32) and 1 μg of pSV-β-Gal (both from Promega) used as an internal control with 9 μg polyethyleneimine. Transfected cells were incubated in medium with various concentrations of DAT for 6 h. Cells were resuspended in 0.1 ml of passive lysis buffer (Promega) for luciferase assays. Luciferase activity was measured with a GloMax 20/20 luminometer. The luciferase activity of DAT-untreated cells was defined as 1.0 relative light unit.

Reverse transcription-polymerase chain reaction (RT-PCR) and real-time RT-PCR. Total RNA was purified and extracted from 1×10^6 cells using an Illustra RNAspin Mini RNA Isolation kit (GE Healthcare, Buckinghamshire, UK). First-strand cDNA was synthesized from 20 ng of total RNA using a ReverTra Ace qPCR RT kit (Toyobo, Osaka, Japan). To quantify cDNA, PCR was performed using GoTaq Flexi DNA polymerase (Promega). The PCR products were analyzed by electrophoresis on 2% agarose gels and staining with ethidium bromide. The nucleotide sequences of oligonucleotides used for RT-PCR primers were as follows: IKKα forward, 5'-AGA CGT CAG GGA GAC TTG ATG-3' and reverse, 5'-ACT GGA TCC TAC AAG AGA GCG-3'; IKKβ forward, 5'-AGG TGC CAT CCT CAC CTT GC-3' and reverse, 5'-AAT GTC CAC CTC ACT CTT CTG CC-3'; IKKγ forward, 5'-AGT TGC AGG TGG CCT ATC ACC-3' and reverse, 5'-CTC ATG TCC TCG ATC CTG GC-3'; TRAF6 forward, 5'-CAG GGG TAT AGC TTG CCC TCA C-3' and reverse, 5'-TGG AAC GTG TGG ATT CCC AG-3'; GAPDH forward, 5'-TGA CCA CAG TCC ATG CCA TC-3' and reverse, 5'-GGG GAG ATT CAG TGT GGT GG-3'.

For quantification of cDNA, Real-time RT-PCR was performed as described previously (10). Briefly, total RNA was purified and extracted from 1×10^6 cells and first-strand cDNA was synthesized from 20 ng of total RNA. To quantify cDNA, SYBR-Green real-time PCR was performed using the MiniOpticon real-time PCR (Bio-Rad, Hercules, CA, USA). The sequences of oligonucleotides used for primers were as follows: IκBα forward, 5'-AGC TTT TGG TGT CCT TGG GTG-3' and reverse, 5'-CTG TTG ACA TCA GCC CCA CAC-3'; RTA forward, 5'-ATA ATC CGA ATG CAC ACA TCT TCC ACC AC-3' and reverse, 5'-TTC GTC GGC CTC TCG GAC GAA CTG A-3'; K8.1 forward, 5'-TCC ACA CAG ATT CGC ACA GA-3' and reverse, 5'-AAT GCG AAC GAT ACG TGG GA-3'. The primer set for GAPDH forward, 5'-GAG TCA ACG GAT TTG GTC GT-3' and reverse, 5'-GAC AAG CTT CCC GTT CTC AG-3' was used as an internal control for normalization. For quantification, the expression level of each gene was normalized to that of the GAPDH gene.

Transfection and plasmids. 293/TLR4-MD2-CD14 (293/TLR4) cells were purchased from InvivoGen (San Diego, CA, USA). The 293 or HeLa cells seeded at 2×10^6 cells/10 cm dish were transfected using the Chen-Okayama calcium phosphate procedure (30) with 10 µg of plasmid, and harvested 48 h after transfection.

The open reading frames (ORFs) of human ubiquitin, IKKα, IKKβ, IKKγ and TRAF6 were amplified by PCR. All constructs were verified by DNA sequencing. For eukaryotic expression, the respective PCR fragments were cloned into the pCI-neo-Flag, pCI-neo-T7, pCI-neo-Myc or pCI-neo-S-tag vector, which had been generated by inserting oligonucleotides encoding three repeats of a Flag-tag sequence, three repeats of a T7-tag sequence, a Myc-tag sequence, and two repeats of an S-tag (S-tag peptide), respectively, into the pCI-neo mammalian expression vector (Promega).

Immunoprecipitation. Immunoprecipitation assays to detect polyubiquitination of IκBα were performed according to the methods described by Saji *et al* (10). BC3 cells (1×10^7) were lysed in 1 ml RIPA buffer. Cell lysates were incubated with 5 µg of anti-IκBα antibody. Immunoprecipitated IκBα was immunoblotted with FK2 (anti-polyubiquitin) or anti-IκBα antibody. Immunoprecipitation assays to detect the interactions of IKKα, IKKβ and IKKγ were performed, as described previously (5).

Measurement of proteasome activity. BC3 cells (1×10^6) were lysed in 0.2 ml of buffer containing 50 mM Tris-HCl (pH 7.6), 1 mM $MgCl_2$, 0.1 mM EDTA, 1% glycerol, 1 mM DTT, 0.2 mM ATP, 0.2% NP-40, and homogenized with 27 G needles and 1 ml disposable syringes. The chymotrypsin-like activity of the proteasome in cell lysate was assessed with the fluorogenic peptide, Suc-Leu-Leu-Val-Tyr-4-methylcoumaryl-7-amide (MCA) (Peptide Institute, Osaka, Japan). The cell lysates (5 µl) were incubated in 95 µl of reaction buffer containing 50 mM Tris-HCl (pH 7.8), 10 mM $MgCl_2$, 1 mM DTT, 2 mM ATP, 0.1 mM Suc-Leu-Leu-Val-Tyr-MCA. The fluorescence intensity owing to AMC (excitation, 380 nm; emission, 460 nm) was determined using a microplate spectrofluorometer (Infinite M200; Tecan, Kawasaki, Japan).

Real-time PCR measurement of viral load. Real-time PCR was performed by the method described previously (10). BCBL1 cells (2×10^5) were treated with 3 mM n-butyrate and DAT for 48 h, and the culture media were harvested. To obtain only enveloped and encapsulated viral genomes, media were incubated with DNase I, and viral DNA was purified using a QIAamp DNA blood mini kit (Qiagen, Hilden, Germany). To quantify viral DNA, SYBR Green real-time PCR was performed by MiniOpticon real-time PCR (Bio-Rad). To generate a standard curve for cycle threshold versus genomic copy number, the pCIneo-KSHV ORF50/RTA plasmid was serially diluted to known concentrations in the range of 10^1-10^6 plasmid molecules/µl. Each PCR mixture contained 1 µl viral or standard DNA, 0.5 µM ORF50 primers, 10 µl SYBR Master Mix Plus (Bio-Rad), and H_2O in a total volume of 20 µl. The following primers were used to amplify a 140-bp amplicon internal to the ORF50 sequence: ORF50/RTA forward, 5'-ATA ATC CGA ATG CAC ACA TCT TCC ACC AC-3' and reverse, 5'-TTC GTC GGC CTC TCG GAC GAA CTG A-3'. The PCR conditions were as follows: 95˚C for 2 min, followed by 95˚C for 5 sec and 62˚C for 20 sec, repeated for 40 cycles.

Xenograft mouse model of PEL. CB17 SCID female mice aged 5 weeks were purchased from CLEA Japan (Tokyo, Japan). Mice were allowed to feed *ad libitum* on sterilized laboratory chow and water. Mice were injected intraperitoneally with 5×10^7 BCBL1 cells before 1 week of DAT administration. The DAT dissolved in corn oil or corn oil alone was administered into the intraperitoneal region at a dose of 5 mg/kg body weight each day for 3 weeks. Mice were observed and body weight was measured each day for 3 weeks. All mice were sacrificed on day 21, and the ascites and organs were collected. The ascites collected from each mouse was centrifuged to determine the tumor weight. Genomic DNA of tumor cells in ascites was purified using SepaGene (EIDIA, Tokyo, Japan) and subjected to real-time PCR to quantify viral DNA. All experiments were carried out in accordance with the Code of Ethics of the World Medical Association (Declaration of Helsinki) and the guiding principles for the care and use of laboratory animals in Kyoto
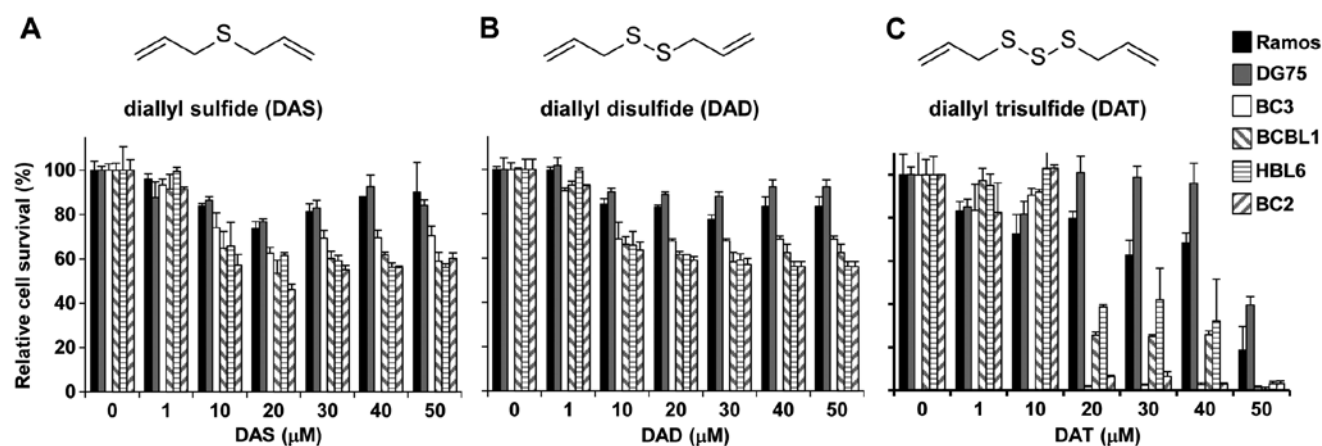
Figure 1. Cytotoxic effects of diallyl sulfide (DAS), diallyl disulfide (DAD), and diallyl trisulfide (DAT) on PEL cells and KSHV-uninfected lymphoma cells. (A-C) Show the structures and cytotoxic effects of DAS, DAD and DAT, respectively. KSHV-positive PEL cells (BC3, BCBL1, BC2 and HBL6 cells) and KSHV-uninfected lymphoma cells (Ramos and DG75 cells) were incubated with various concentrations of DAS, DAD, and DAT for 24 h and subjected to cell viability assays. For each cell type, viability was assessed in three replicate wells. The optical density at 450 nm was measured, and the values of the respective untreated cells were defined as 100%. Standard deviations were determined by analysis of data from three independent experiments, and are indicated by error bars.

Table I. Cytotoxic effects of DAT on B-lymphoma cells.

	BC3	BCBL1	HBL6	BC2	Ramos	DG75
CC_{50} (μM)	13.7±0.8	15.5±1.0	17.7±0.6	14.6±0.4	43.4±1.4	48.0±0.9

CC_{50}, cytotoxic concentration of DAT that reduces cell viability by 50%.

Pharmaceutical University (KPU). Animal studies were approved by the Experimental Animal Research Committee at KPU.

Results

Cytotoxic effects of DAT on PEL cells. First, we examined the cytotoxic effects of allyl sulfides (DAS, DAD and DAT) on KSHV-infected PEL cell lines (BC3, BCBL1, HBL6 and BC2) and KSHV-uninfected lymphoma cell lines (Ramos and DG75). These B-lymphoma cells were cultured in the presence of DAS, DAD or DAT for 24 h, and the cytotoxicity was evaluated by analyzing the viability of allyl sulfide-treated versus untreated cells (Fig. 1). DAS and DAD treatments slightly decreased the viability of PEL cells compared to KSHV-uninfected cells (Fig. 1A and B) whereas DAT treatment selectively prevented the proliferation of PEL cell lines at lower concentrations than required for KSHV-uninfected Ramos and DG75 cell lines (Fig. 1C). In particular, treatment with 20 μM DAT showed marked antiproliferative effects on PEL cell lines with no influence on KSHV-uninfected cell lines. The cytotoxic effects of DAT on B-lymphoma cells are summarized in Table I. As DAT showed strong antiproliferative activities against PEL, we focused on the cytotoxic effects of DAT and analyzed the underlying molecular machinery.

DAT induces apoptosis through the activation of caspases in PEL cells. We next investigated whether the cytotoxic effects of DAT were due to apoptotic cell death. Apoptosis is induced by the activation of executioner caspases, including caspase-3 and

-7, which have been previously activated via either an intrinsic pathway (caspase-9) or an extrinsic pathway (caspase-8). We monitored the cleavage (i.e., activation) of caspase-3, -7, -8 and -9 by immunoblotting of lysates prepared from PEL and Ramos cells cultured with DAT (Fig. 2A). Active caspase-3, -7 and -9 were detected in BC3 and BCBL1 cells that had been treated with DAT for 6 and 12 h. Further, the amounts of cleaved PARP were increased in DAT-treated BC3 and BCBL1 cells. However, on immunoblotting analysis, active caspase-8 was slightly detected in BC3 and BCBL1 cells. In contrast, neither the cleavage of caspase nor the accumulation of cleaved PARP was detected in DAT-treated Ramos cells. In addition to the activation of caspase, p21^{Cip1} was upregulated in DAT-treated cells. To obtain further evidence of the activation of caspase-9, we measured the peptidase activities of caspase-8 and -9 in BC3 cells pretreated with DAT (Fig. 2B). Compared to treatment with vehicle control, treatment with DAT increased caspase-8 and -9 activities by 1.2- and 1.6-fold, respectively. There was no significant difference in caspase-8 between DAT-treatment and control. These data indicate that DAT inhibited the growth of PEL cells by cell cycle arrest, leading to caspase-9-dependent apoptosis. We adopted different treatment times and drug concentrations as shown in Fig. 2. The reasons of treatment times are as follows. Activations of executioner caspases (caspase-3 and -7) and PARP cleavage occur later in the apoptosis cascade, while activations of initiator caspases (caspase-9 and -8) occur early in the apoptosis. In fact, strong activation of caspase-9 and PARP cleavage were detected in cells treated with DAT for 6 and 12 h, respectively (Fig. 2A). Regarding drug concentrations, more DAT were necessary for
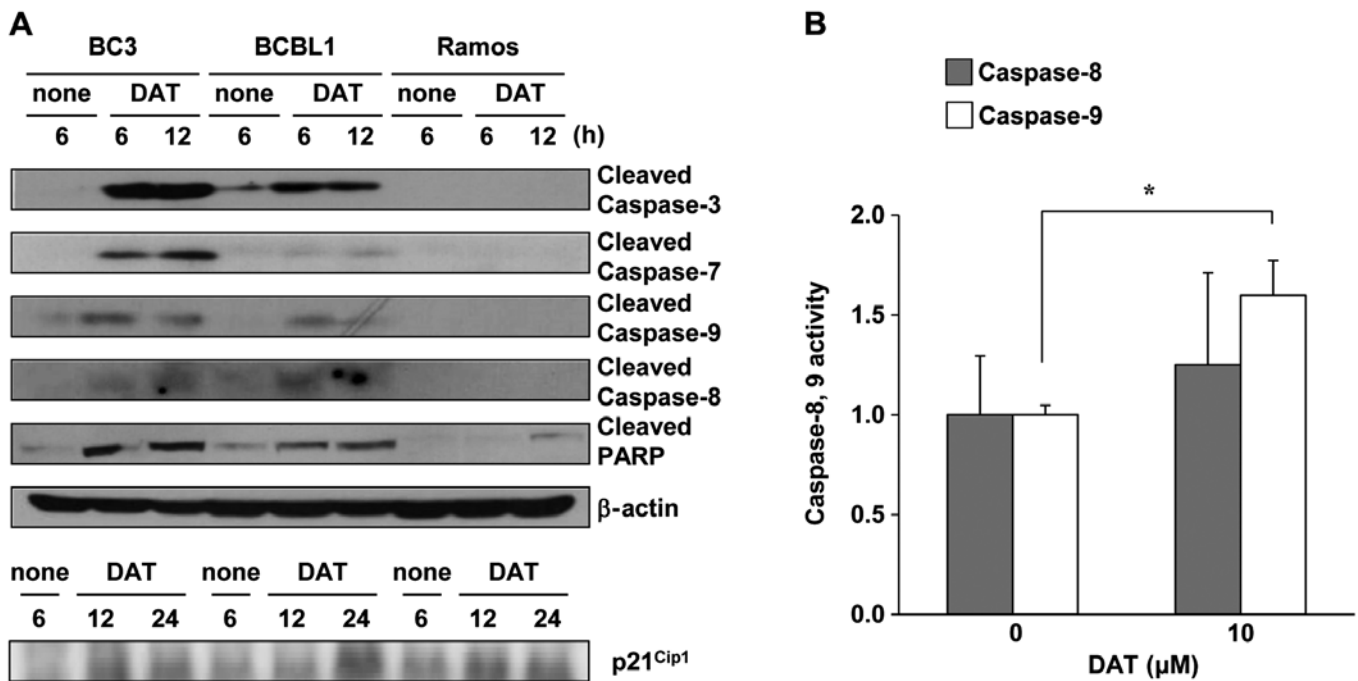
Figure 2. Apoptosis-inducing effect of DAT on PEL cells. (A) Activation of caspase-3, -7 and -9 in DAT-treated PEL cells. PEL (BC3 and BCBL1) and KSHV-uninfected lymphoma Ramos cells were cultured with 20 μM DAT for 6, 12 or 24 h. Untreated cells were cultured without DAT for 6 h. Cell lysates were subjected to western blotting. (B) Changes in the activities of caspase-8 and -9 in DAT-treated BC3 cells. BC3 cells were treated with or without 10 μM DAT for 3 h before harvesting. The activity of caspase-8 or -9 was measured by the caspase-Glo assay using luciferin-conjugated LETD or LEHD polypeptide substrate, respectively. Caspase activity in untreated cells was defined as 1.0 relative light unit (RLU). The error bars indicate the standard deviation of three independent experiments. *p<0.05 (t-test).

western blotting to detected cleaved molecules (i.e., activated forms) because western blot analysis has low detection sensitivity as compared with peptidase assay.

DAT suppresses NF-κB signaling through the stabilization of IκBα. Several signaling pathways are activated in PEL cells to maintain malignant potential and enhance cell survival. Especially, the constitutive and/or transient activation of NF-κB signaling is necessary for PEL to achieve the establishment of KSHV infection, survival of infected cells, and viral replication (4,7-11). To obtain insight into the machinery by which DAT induces apoptosis of KSHV-infected PEL cells, we analyzed the effect of DAT treatment on NF-κB signaling. PEL and KSHV-uninfected Ramos cells were incubated in medium with 10 μM DAT, expression of IκBα was elucidated by western blot analysis. DAT treatment significantly increased the expression of IκBα in PEL cells, whereas, upregulation of IκBα was not detected in Ramos cells (Fig. 3A). The long exposure image is shown, indicating the IκBα upregulation in BC3 treated with DAT for 6 and 12 h. To determine whether DAT-mediated upregulation of IκBα is due to transcriptional activation of IκBα, we measured the expression of IκBα mRNA in PEL cells treated with DAT by real-time RT-PCR (Fig. 3B). The result indicated that DAT treatment had no influence on IκBα mRNA in BCBL1, suggesting that DAT induces the stabilization of IκBα. As DAT showed increased expression of IκBα, we next examined the suppression of NF-κB nuclear translocation and the downregulation of NF-κB-dependent transcriptional activity by DAT treatment. IF analysis showed that compared to untreated controls, DAT treatment induced cytosolic localization of p65 in BCBL1 cells (Fig. 3C). The amount of p65 in the nucleus decreased in BC3 and BCBL1 cells treated with DAT for 12 and 24 h (Fig. 3D), as compared to Ramos cells, while DAT did not alter the total amount of p65 in all cell lines (Fig. 3D). In addition, we performed a reporter assay using the NF-κB reporter plasmid to confirm the suppression of NF-κB in BC3 cells by DAT-treatment. As expected, DAT treatment suppressed NF-κB transcriptional activity of BC3 cells in a concentration-dependent manner (Fig. 3E). Western blot analysis for detection of immunoprecipitated IκBα using lysates from DAT-treated BC3 and BCBL1 is also shown. Data show that DAT-treatment for 6 h significantly induced IκBα upregulation in PEL cells. These data indicated that DAT treatment suppressed NF-κB signaling through the stabilization of IκBα in PEL cells.

DAT induces stabilization of IκBα by inhibiting phosphorylation of IκBα. The mechanism of IκBα degradation consists of three sequential steps: first, the phosphorylation of IκBα by IKK complex; second, polyubiquitination of phosphorylated IκBα by E3 ubiquitin ligase; and third, degradation of polyubiquitinated IκBα by 26S proteasome. We attempted to determine which step is influenced by DAT treatment, leading to the stabilization of IκBα. First, we monitored polyubiquitination of IκBα (Fig. 4A). To detect polyubiquitination of IκBα, immunoprecipitated IκBα from DAT and MG132-treated BC3 cell lysate was subsequently probed by immunoblotting with an anti-polyubiquitin antibody (FK2). However, there was no difference in amount of polyubiquitination of IκBα between
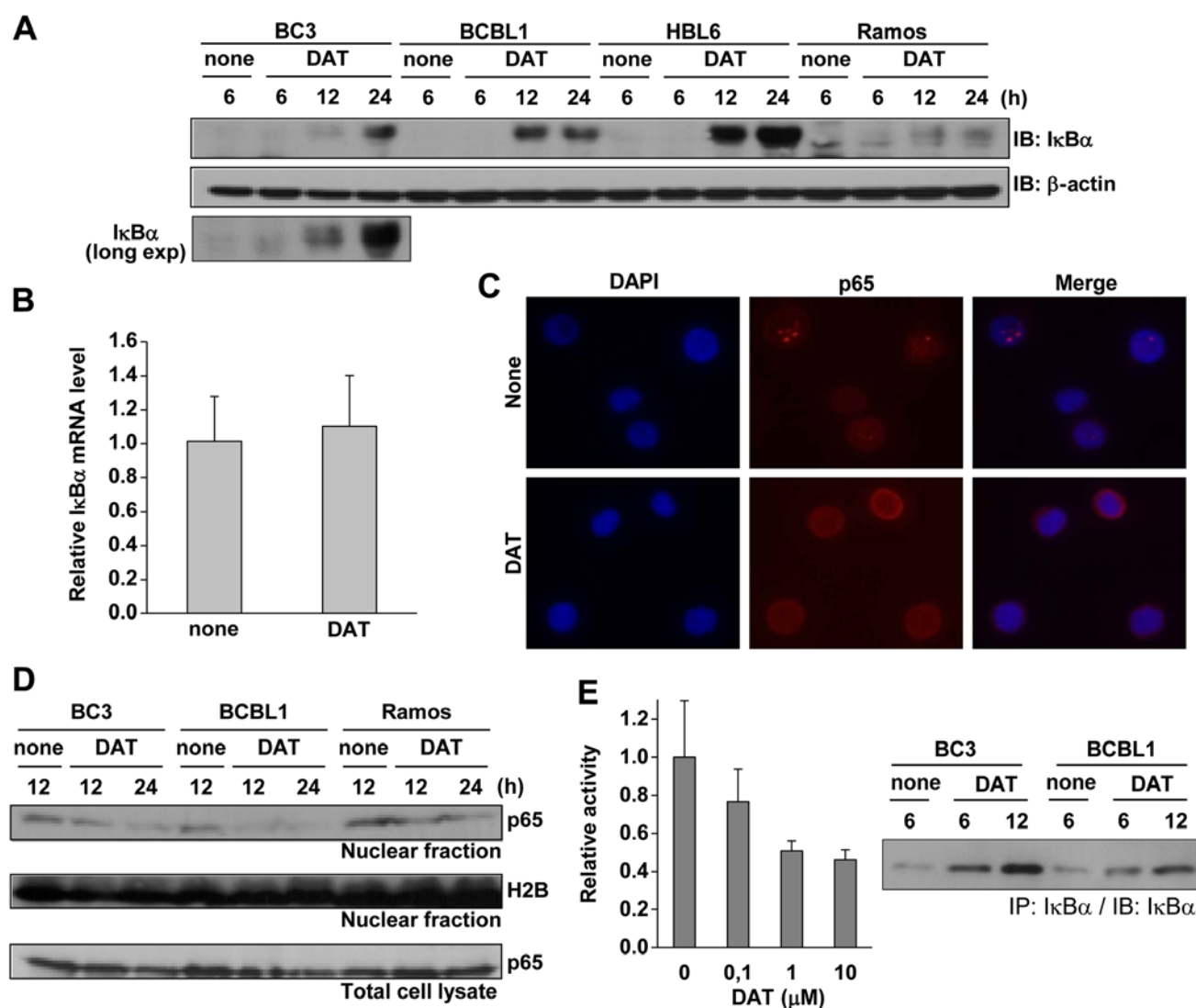
Figure 3. Suppression of NF-κB signaling through IκBα stabilization by DAT. (A) DAT-induced IκBα expression in PEL cells. PEL (BC3, BCBL1 and HBL6) and Ramos cells were cultured in the presence or absence of 10 μM DAT and then harvested. To quantify IκBα, whole-cell lysates were analyzed by immunoblotting with an anti-IκBα antibody. The lower panel is the long exposure image of IκBα blotting using BC3 samples. (B) Effects of DAT on IκBα mRNA expression in PEL cells. BCBL1 cells were cultured with 20 μM DAT for 6 h, and total RNA extracted from cells was subjected to real-time RT-PCR. (C) Immunofluorescence analysis using anti-p65 antibody. BCBL1 cells were cultured with 10 μM DAT for 18 h and fixed in ice-cold methanol. The fixed cells were incubated with anti-p65 (red) antibody and DAPI to stain the nuclei (blue). (D) DAT-dependent inhibition of NF-κB nuclear translocation in PEL cells. Cells were cultured with 10 μM DAT. Nuclear fractions were prepared from harvested cells, and NF-κB (p65/RelA) nuclear translocation was analyzed by immunoblotting. (E) Inhibition of NF-κB transcriptional activity by DAT. BC3 cells were transfected with the NF-κB reporter plasmid. Transfected cells were treated with various concentrations of DAT for 6 h and lysed in buffer for luciferase assay. The NF-κB activity of untreated BC3 cells was defined as 1.0 relative activity. The right panel shows western blotting for detecting immunoprecipitation (IP) of IκBα using BC3 and BCBL1 cells treated with 10 μM DAT for 6 h. Cell extracts were subjected to IP with anti-IκBα antibody, and precipitates were examined by blotting with anti-IκBα antibody.

DAT-treated and untreated cells. Next, to examine whether DAT inhibited the degradation of IκBα by the 26S proteasome, we measured the chymotrypsin-like activity of the proteasome. In BC3 cells treated with DAT for 24 h, the proteasome activity decreased by ~20% compared to that in untreated cells (Fig. 4B). The proteasome inhibitor MG132 was used as a positive control. We also investigated the effects of DAT on IκBα phosphorylation in PEL cells. When BC3 cells were treated with DAT, the amount of phosphorylated IκBα (p-IκBα) protein was significantly decreased compared to untreated cells (Fig. 4C). BAY11-7082, which inhibits IKK and IκB phosphorylation, was used as a positive control. We evaluated the cytotoxic effect of BAY11-7082 on PEL to confirm the contribution of IκBα phosphorylation to apoptotic activity

on PEL. Treatment with BAY11-7082 markedly decreased the viability of BC3 PEL cells compared to KSHV-uninfected BJAB cells (Fig. 4D). Thus, our data demonstrated that DAT stabilized IκBα through inhibition of IκBα phosphorylation. Furthermore, DAT-mediated suppression of NF-κB signaling through inhibition of IκBα phosphorylation can be a trigger for apoptosis of PEL cells.

DAT suppresses the phosphorylation of IKKβ through down-regulation of TRAF6. We demonstrated that DAT stabilized IκBα through inhibition of IκBα phosphorylation in PEL cells. To determine whether DAT-mediated phosphorylation of IκBα is due to quantitative or qualitative changes in IKK, we examined the mRNA expression, complex formation and
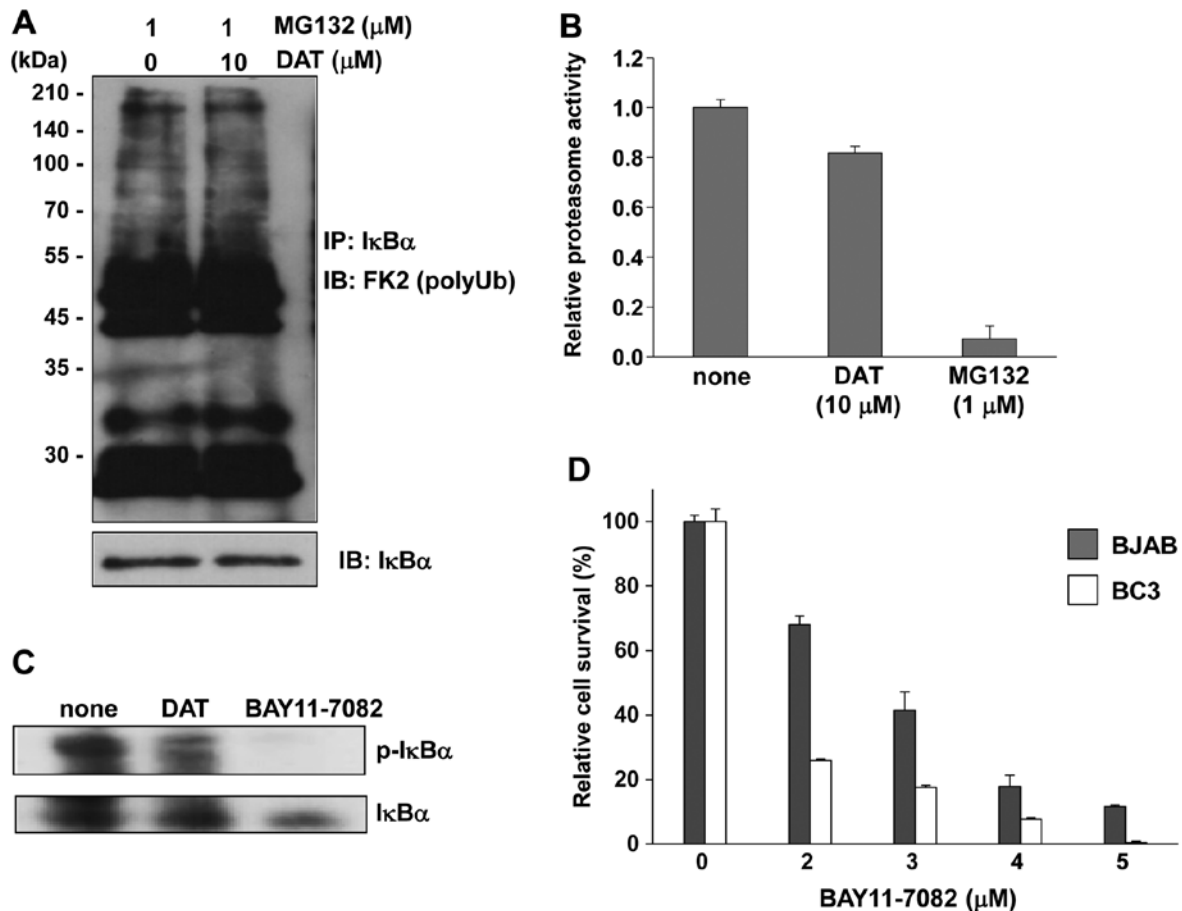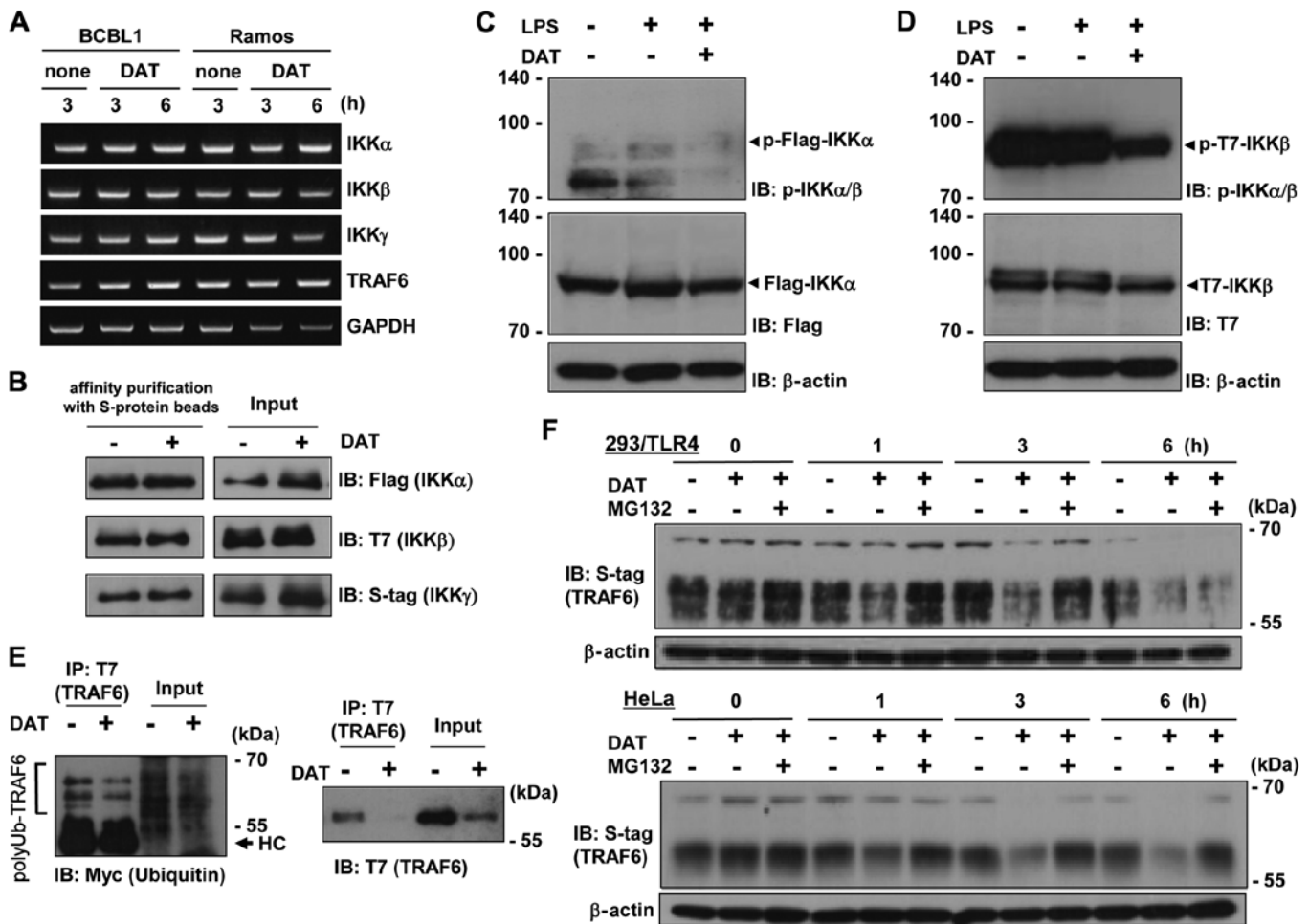
Figure 4. Inhibition of the phosphorylation of IκBα by DAT. (A) Influence of DAT on polyubiquitination of IκBα in PEL cells. BC3 cells were incubated with 10 μM DAT and 1 μM proteasome inhibitor (MG132) for 24 h. To detect polyubiquitination of IκBα, immunoprecipitated IκBα protein was subjected to immunoblotting using FK2, an anti-polyubiquitination antibody. (B) Influence of DAT on the chymotrypsin-like activity of the proteasome in PEL cells. BC3 cells were cultured with 10 μM DAT or 1 μM MG132 for 24 h. The chymotrypsin-like activities of cell lysates were evaluated by fluorometric assay using the synthetic peptide. The proteasome activity of untreated cells was defined as 100%. (C) Immunoblotting of IκBα and phospho-IκBα using DAT-treated BC3 cells. Cells were cultured with or without 10 μM DAT or 0.2 μM BAY11-7082 for 24 h. To detect phosphorylation of IκBα, cell lysates were subjected to blotting using anti-Ser32/36-phospho-IκBα antibodies. To equalize the amounts of IκBα among all samples, 40 μl of none-treated, 10 μl of DAT-treated, and 5 μl of BAY-treated cell lysates were applied to SDS-PAGE. (D) Cytotoxic effects of BAY11-7082 on BC3 and KSHV-uninfected BJAB cells. Cells were incubated with various concentrations of BAY11-7082 for 24 h. Cell viability in inhibitor-untreated cells was defined as 100%.

phosphorylation state of IKK in DAT-treated PEL. The results indicated that DAT treatment did not affect the levels of IKKα, IKKβ or IKKγ mRNA in BCBL1 or Ramos cells (Fig. 5A). We next examined the complexation of IKK in DAT-treated cells. HeLa cells were transfected with Flag-IKKα, T7-IKKβ and S-tag-IKKγ expression plasmids, and treated with DAT. Cell lysates were subjected to coprecipitation assay using S protein-immobilized beads. However, there were no changes in complex formation of IKK associated with DAT treatment (Fig. 5B). Next, we examined whether DAT suppresses the phosphorylation of endogenous IKKα or IKKβ in PEL, HeLa and 293 cells. However, we could not detect the phosphorylation signal of endogenous IKKα/β, because the phosphorylation and expression levels of IKKα/β in normal cultured cells were too low. Therefore, we used 293/TLR4 cells constitutively expressing TLR4. 293/TLR4 cells transfected with either Flag-IKKα or T7-IKKβ cultured with or without DAT-containing medium in the presence of LPS to activate the NF-κB signal. When Flag-tagged IKKα-transfected cells were treated with LPS, small amounts of Ser176 in exogenous IKKα were phosphorylated, and DAT

treatment suppressed this phosphorylation (Fig. 5C). On the contrary, in T7-tagged IKKβ-transfected cells, large amounts of IKKβ were phosphorylated in an LPS-independent manner, and DAT treatment strongly suppressed the phosphorylation of Ser180 at T7-IKKβ (Fig. 5D). That is, DAT suppressed the IKK complex by inhibiting the phosphorylation of IKKβ, which is the catalytic subunit of the IKK complex and directly phosphorylates IκBα for degradation. As the ubiquitin ligase, TRAF6, which is self-activated by TRAF6 polyubiquitination, induces IKKβ phosphorylation via activation of TAK1-TAB2 complex, we compared the self-polyubiquitination of TRAF6 in the presence or absence of DAT. HeLa cells transfected with T7-TRAF6 and Myc-ubiquitin were cultured with or without DAT, and cell extracts were assayed by coimmu-noprecipitation assay. Immunoprecipitated T7-TRAF6 was immunoblotted with anti-T7 and anti-Myc antibody to detect TRAF6 and polyubiquitinated TRAF6, respectively. DAT treatment slightly reduced the polyubiquitination of TRAF6 (Fig. 5E, left panel), but significantly reduced the amount of TRAF6 protein (Fig. 5E, right panel). Therefore, we compared the destabilization of TRAF6 in the presence or absence of

Figure 5. Inhibition of IKKα phosphorylation through destabilization of TRAF6 by DAT. (A) RT-PCR to measure the mRNA expression of IKKα, IKKβ, IKKγ and TRAF6 in DAT-treated PEL. Cells were cultured with 20 μM DAT for 3 or 6 h, and the mRNA were detected from extracted total RNA by RT-PCR. (B) Influence of DAT on IKK complex (IKKα-IKKβ-IKKγ) formation. HeLa cells were transfected with Flag-IKKα, T7-IKKβ and S-tag-IKKγ plasmids and cultured for 24 h. Transfected cells were treated with or without 10 μM DAT for 24 h. The cell extracts were subjected to affinity purification using S-protein-immobilized agarose beads, and purified proteins (S-tag-IKKγ) were subjected to western blotting. (C) Inhibition of IKKα phosphorylation by DAT. 293/TLR4 cells were transfected with 6 μg of Flag-IKKα expression plasmid. Twenty-four hours after transfection, cells were treated with or without 20 μM DAT for 6 h in DMEM containing 40 ng/ml lipopolysaccharide (LPS). Harvested cells were subjected to immunoblotting using anti-Ser176/180 phospho-IKKα/β antibody to detect Ser176-phosphorylated Flag-IKKα. The anti-Ser176/Ser180 phospho-IKKα/β antibody recognizes Ser176-phosphorylated IKKα and Ser180-phosphorylated IKKβ. (D) Inhibition of IKKβ phosphorylation by DAT. 293/TLR4 cells were transfected with T7-IKKβ, and cells were treated with DAT and LPS for 6 h. Cells were subjected to immunoblotting using anti-Ser176/180-phospho-IKKα/β to detect Ser180-phosphorylated T7-IKKβ. (E) Effect of DAT on polyubiquitination of TRAF6. HeLa cells were transfected with 3 μg of T7-TRAF6 and 3 μg of Myc-ubiquitin (Ub) expression plasmids, and cultured with 20 μM DAT in DMEM for 24 h. Cell extracts were incubated with 10 μl of anti-T7 antibody-immobilized agarose beads for 1 h. To detect polyubiquitination of TRAF6, immunoprecipitates (T7-TRAF6) were subjected to SDS-PAGE followed by blotting with anti-T7 (to detect TRAF6) and Myc (to detect polyubiquitin) mouse antibodies. The arrowhead indicates Ig heavy chain. (F) Proteasome-dependent destabilization of TRAF6 by DAT. 293/TLR4 or HeLa cells were transfected with 6 μg of S-tag-TRAF6 and cultured for 24 h. Transfected cells were cultured with 20 μM DAT and 10 μM MG132 in DMEM containing 25 μg/ml cycloheximide for 0, 1, 3 or 6 h, and lysed in SDS-PAGE sample buffer. To determine the amount of TRAF6 protein, lysates of 293/TLR4 (upper panel) or HeLa cells (lower panel) were analyzed by immunoblotting using an anti-S-tag rabbit polyclonal antibody.

DAT. S-tag-TRAF6-transfected 293/TLR4 or HeLa cells were incubated with DAT, and TRAF6 was detected by immunoblotting with an anti-S-tag antibody. The results indicated that DAT treatment for 3 and 6 h induced destabilization of TRAF6 in 293/TLR4 (Fig. 5F, upper panel) and HeLa cells (Fig. 5F, lower panel). In addition, the proteasome inhibitor, MG132, overcame the DAT-induced destabilization of TRAF6. In Fig. 5A, we confirmed that DAT did not affect the expression of TRAF6 mRNA in cells. These data indicate that DAT induces degradation of TRAF6 by the proteasome, and DAT-mediated downregulation of TRAF-6 suppresses the phosphorylation of IKKβ and activation of IKK complex. Furthermore, DAT-mediated suppression of IKK induces the

suppression of IκBα phosphorylation for polyubiquitination and proteasomal degradation of IκBα.

DAT inhibits KSHV replication in PEL. NF-κB signaling is essential for replication of KSHV (10,11). Therefore, we investigated whether DAT suppresses KSHV lytic replication in PEL cells (Fig. 6A). The results showed that DAT suppressed viral particle production at low concentrations, which did not affect BCBL1 cell growth (Fig. 1). Next, to investigate which step of viral replication is prevented by DAT we examined the effect of DAT on lytic gene expression for viral replication. DAT treatment decreased mRNA expression of RTA (immediate-early gene) and K8.1 (late gene) in BCBL1 cells
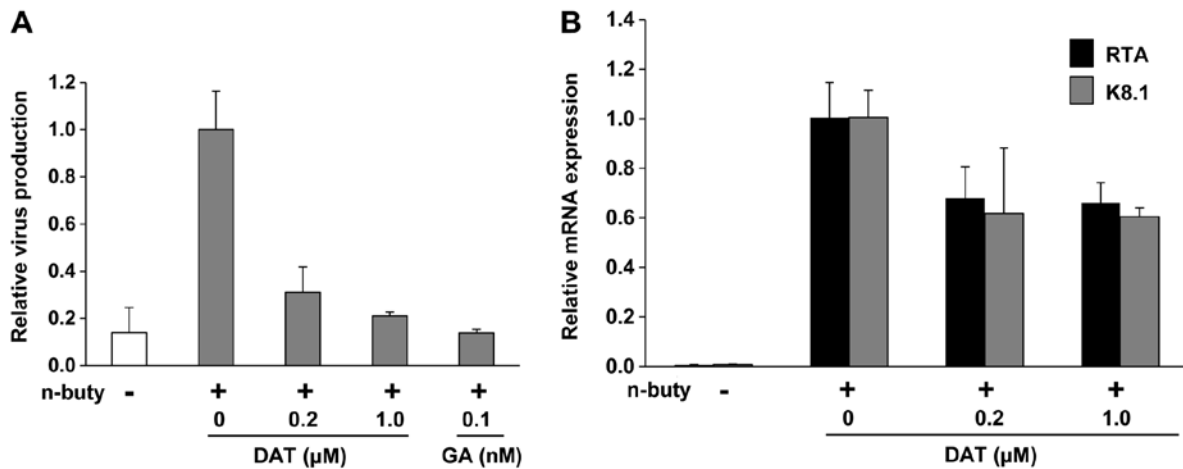
Figure 6. Effects of DAT on lytic replication in BCBL1 cells. (A) Suppression of KSHV replication by DAT. BCBL1 cells were cultured for 24 h with DAT in RPMI medium containing 3 mM n-butyrate for induction of KSHV lytic replication. The Hsp90 inhibitor, geldanamycin (GA), was used as a positive control for inhibition of lytic replication (11). Culture medium containing virus particles was harvested and KSHV genome copy numbers were quantified by real-time PCR. The KSHV genome copy number in DAT-untreated BCBL1 cells induced by n-butyrate was defined as 1.0. (B) The effects of DAT on mRNA expression of the lytic genes, RTA/ORF50 and K8.1. BCBL1 cells were treated for 24 h with 0, 0.2 or 1.0 μM DAT in the presence of 3 mM n-butyrate. Total RNA was extracted from harvested cells and subjected to real-time RT-PCR. The levels of respective gene expression in DAT-untreated BCBL1 cells induced by n-butyrate were defined as 1.0.

lytically induced by n-butyrate (Fig. 6B). DAT treatment was suggested to influence the early stage of KSHV replication, i.e., viral gene transcription, in PEL cells. These results indicate that NF-κB activity is required for both KSHV-infected cell survival and viral replication in PEL cells.

Treatment with DAT suppresses the development of PEL in SCID mice. As DAT showed selective cytotoxicity on PEL cell lines (Fig. 1), we next investigated whether DAT treatment exerted cytotoxic effects against xenograft PEL cells in SCID mice. BCBL1 cells were injected intraperitoneally into SCID mice 1 week prior to commencement of DAT administration. DAT or vehicle (corn oil) was injected intraperitoneally each day for 21 days. The mice with and without DAT administration showed significantly different gross appearance (Fig. 7A): the abdomen of corn oil-treated PEL-xenografted mice (control mice) showed expansion, whereas DAT-treated mice had an apparently normal body shape. Moreover, the body-weight increase of DAT-treated mice was less marked than that of control mice (Fig. 7B). Necropsy revealed that the spleens of control mice showed distention compared to those of DAT-treated mice (Fig. 7C), whereas there were no significant morphological differences in other organs between DAT-treated and -untreated mice. The weight of the spleen in the DAT-treated group was ~0.07 g, which was lower than that of the corn oil-treated group (Fig. 7D). As the average weight of the spleen in normal 6-7-week-old SCID mice is ~0.06 g (data not shown), the spleens of control mice were considerably larger than those of normal and DAT-treated mice. The weight of tumor cells in ascites in the DAT-treated group was significantly less than that of control group (Fig. 7E). Real-time PCR indicated that ascites and spleen tumor cells were infected with KSHV in corn oil-treated mice, and DAT treatment markedly decreased KSHV DNA in ascites and spleen compared to control (Fig. 7F and G). IF analysis showed that the tumor cells in ascites from control mice expressed LANA, a marker of latent KSHV infection (Fig. 7H). These

results indicated that xenografted BCBL1 developed in ascites of corn oil-treated control mice, and DAT prevented BCBL1 development in ascites.

Discussion

Our data showed that DAT exhibited the greatest cytotoxicity against PEL among the allyl sulfides (DAS, DAD and DAT) tested in this study (Fig. 1). DAT specifically inhibited the growth of PEL cell lines compared with KSHV-uninfected cells both *in vitro* and *in vivo* (Figs. 1C and 7). DAS, DAD and DAT have antitumor effects, but DAS has been shown to have antioxidant and protective effects against oxidative or chemical stress rather than cytotoxic effects (31). On the other hand, DAD and DAT show cytotoxic rather than cell-protective effects. In particular, DAT was shown to induce apoptosis in cancer cells by the generation of ROS and the dysregulation of signaling pathways, including Bcl2-caspase-9, Erk, Jnk and Akt signaling (32,33). By cleavage within its trisulfide bonds, DAT generates ROS, leading to ER stress and apoptotic cell death (20-23,34). In addition, DAT has been reported to suppress NF-κB and to induce apoptosis, DAT reduced LPS-induced NF-κB transcriptional activation in macrophages (35), and DAT suppressed high-glucose-induced apoptosis by inhibiting NF-κB signaling via decreases in nuclear translocation of NF-κB (36). Furthermore, DAT suppressed NF-κB through an increase in IκBα in osteosarcoma cells, resulting in a decrease in P-glycoprotein (37). DAT suppresses dextran sodium sulfate-induced mouse colitis by inducing STAT3 phosphorylation and suppression of IκBα phosphorylation (24). However, the detailed mechanism by which DAT inhibits NF-κB signaling has not been determined. To our knowledge, this is the first report of the detailed mechanism of dysregulation of NF-κB signaling by DAT. Thus, DAT has the ability to interfere in cell signaling including NF-κB, while constitutive and/or transient activation of NF-κB, Akt and Erk signaling are necessary for PEL to enhance cell growth and survival (4-11). These findings
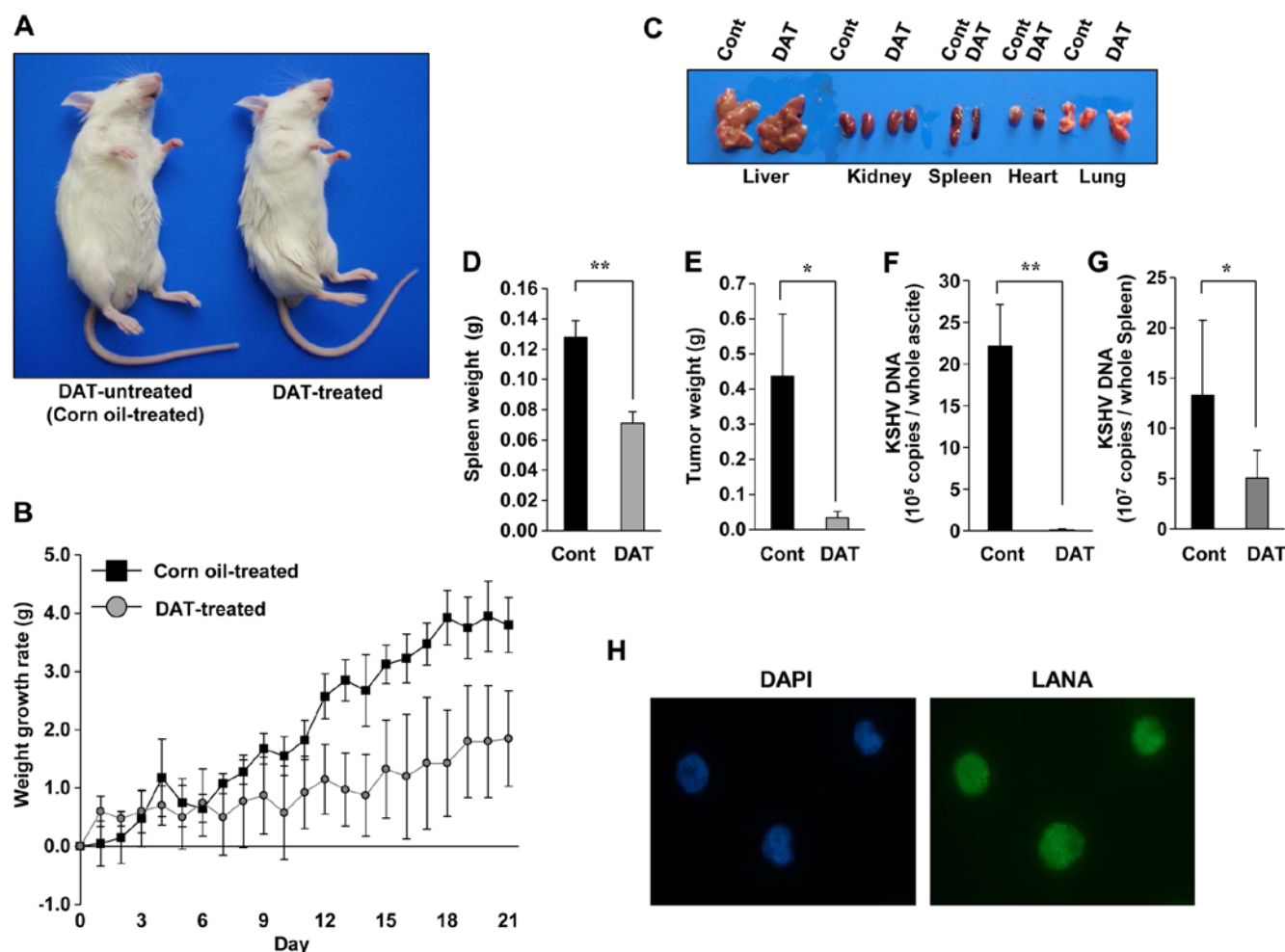
Figure 7. *In vivo* effects of DAT on development of PEL cells in SCID mice. (A) Photograph showing DAT-treated (right) and DAT-untreated (left) SCID mice on day 21 after commencement of DAT administration. SCID mice were injected intraperitoneally with 5×10^7 BCBL1 cells 1 week before commencement of DAT administration. DAT dissolved in corn oil (DAT-treated) or corn oil alone (DAT-untreated) was administered intraperitoneally at a dose of 5 mg/kg body weight each day for 21 days. (B) The body weight changes of BCBL1-xenografted SCID mice for 3 weeks every day from commencement of intraperitoneal DAT or corn oil administration. The body weight changes of untreated mice (n=4) are indicated by black squares, and those of DAT-administered mice (n=4) are indicated by gray circles. At least four mice were tested for each experiment, and the error bars represent the standard deviations. (C) Photograph of the liver, kidney, spleen, heart and lung of DAT-treated and DAT-untreated BCBL1-xenografted mice. Individual organs from DAT-untreated mice (Cont) and DAT-treated mice (DAT) are on the left and right, respectively. (D) Spleen weight of DAT-untreated or DAT-treated BCBL1-xenografted SCID mice. The weight (Cont) of the spleen from DAT-untreated BCBL1-injected mice is indicated by black bars and that (DAT) from DAT-treated BCBL1-injected mice is indicated by gray bars. (E) The weight of intraperitoneal tumor cells of DAT-untreated (Cont) or DAT-treated (DAT) BCBL1-administered SCID mice. Tumor weights of DAT-untreated mice (n=4) and DAT-treated mice are indicated by black and gray bars, respectively. Ascites containing tumor cells were collected from each mouse on day 21 after the first DAT administration. Tumor cells were separated from ascites by centrifugation, and tumor weight was measured. The wet weight of the obtained precipitate was regarded as the tumor weight. (F) KSHV genome of tumor cells in ascites from DAT-untreated (Cont) or DAT-treated (DAT) BCBL1-administered mice. The KSHV genome copy numbers from ascites cells were quantified by real-time PCR. (G) KSHV genome of the spleens from DAT-untreated (Cont) or DAT-treated (DAT) BCBL1-administered mice. The KSHV DNA copy numbers in the spleen were quantified by real-time PCR. (H) LANA expression of ascites cells from DAT-untreated BCBL1-administered mice. The intraperitoneal tumor cells were collected from ascites of DAT-untreated xenografted mice, and were fixed in methanol, followed by incubation with anti-LANA antibody. (D-H) Ascites cells and spleen were collected from BCBL1-xenografted SCID mice on day 21 after the first DAT or corn oil administration. Standard deviations were determined by analysis of data from three independent mice. *p<0.05 and **p<0.01 (t-test).

may be a reason why DAT, rather than DAS and DAD, showed selective cytotoxic effect on PEL cells.

The present study revealed a novel biological function of DAT and a mechanism for DAT-mediated NF-κB suppression. We propose a model in which TRAF6 downregulation by DAT results in suppression of NF-κB signaling (Fig. 8). DAT induced the proteasomal degradation of TRAF6, and this DAT-mediated TRAF6 downregulation suppressed IKKβ phosphorylation (Fig. 5), resulting in inhibition of the IKK complex. The suppression of the IKK complex by DAT decreased the Ser32

and Ser36 phosphorylation of IκBα (Fig. 4C) followed by stabilization of IκBα in a DAT-dependent manner (Fig. 3A). DAT induced stabilization of IκBα by these molecular mechanisms, and then suppressed both the nuclear localization of p65 and the transcriptional activity of NF-κB in PEL cells (Fig. 3); in contrast, DAT did not affect the stabilization of IκBα in KSHV-uninfected cells. It has been suggested that TRAF6 induces the activation of IKK complex and TAK1-TAB2 complex via K63-linked polyubiquitin (12-14). TRAF6, an E3 ubiquitin ligase, catalyzes synthesis of K63-linked polyu-
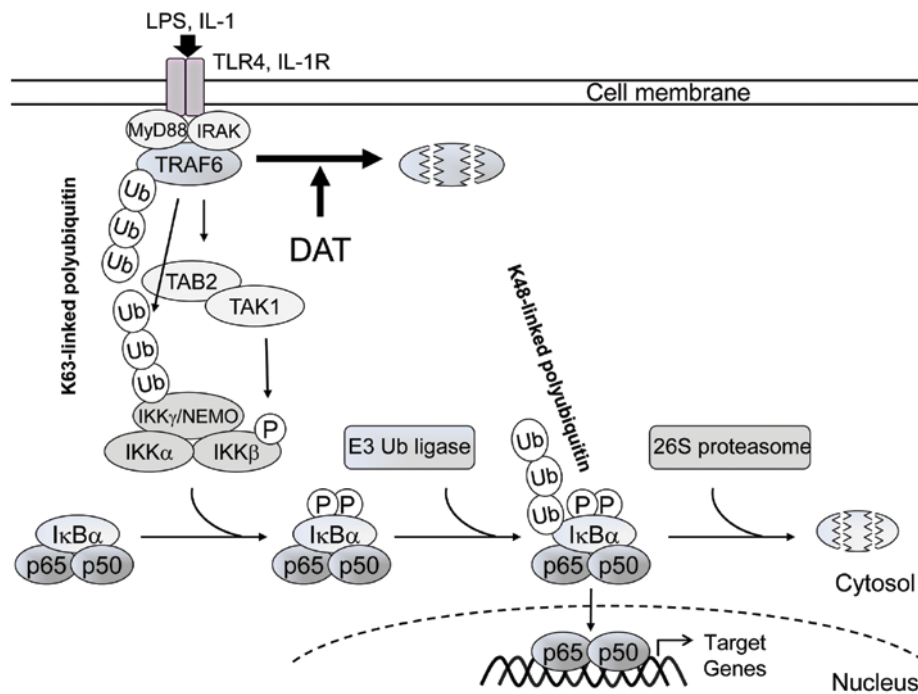
Figure 8. Model of DAT-mediated inhibition of NF-κB signaling. TRAF6 modifies IKKγ and TRAF6 itself with K63-linked polyubiquitin. The K63-linked polyubiquitination of IKKγ and TRAF6 has been shown to contribute the activation of the TAK1-TAB2 complex. Activated TAK1 phosphorylates IKKβ and activates the IKK complex. Polyubiquitinated IKKγ also contributes to the activation of the IKK complex. Activated IKK complex phosphorylates IκBα, and phosphorylated IκBα is modified with K48-linked polyubiquitin, leading to degradation of IκBα and release of NF-κB from IκBα. DAT induces proteasome-dependent downregulation of TRAF6, and suppresses IKKβ phosphorylation, leading to stabilization of IκBα. This DAT-mediated IκBα stabilization suppresses NF-κB-dependent gene expression.

biquitination of IKKγ and TRAF6 itself (12). The K63-linked polyubiquitin chains function as a scaffold to recruit the TAK1-TAB2 complex and IKK complex through binding to TAB2 and IKKγ, respectively (13). Recruitment of the kinase complexes facilitates phosphorylation of the catalytic subunit IKKβ by TAK1, leading to activation of IKK complex. The activated IKK complex induces phosphorylation of IκBα, which acts as a trigger for K48-linked polyubiquitination by SCF-type E3 ubiquitin ligase (38), and the subsequent proteasomal degradation of IκBα. TRAF6 has the RING domain for binding E2, and has been classified as a monomeric RING-type E3 ubiquitin ligase. TRAF6 interacts with Ubc13, which is one of the E2s, forms a dimer with Uev1A (also called Mms2), and mediates the K63-linked polyubiquitination of IKKγ and TRAF6 itself (13,39). The functions of TRAF6 are not aimed at targeting proteins for degradation, but to induce qualitative changes in polyubiquitinated proteins, including stabilization (40), changing localization (41), and signal cascade activation (13,14). It has been suggested that K63-linked self-polyubiquitination of TRAF6 is important for signal transduction from TRAF6 to downstream effectors, such as IKKγ or TAK1-TAB2 complex. It is demonstrated that DAT induces the proteasome-dependent degradation of TRAF6, leading to suppression of NF-κB signaling. This suggests that DAT may induce malformation or disorder of TRAF6-Ubc13-Uev1A complex, resulting in K48-linked self-polyubiquitination of TRAF6 and subsequent TRAF6 degradation by the 26S proteasome. It is possible that additional consequences of DAT-induced TRAF6 degradation will become apparent upon further characterization of additional participants in the TRAF6 complex in the presence of DAT.

We propose that the PEL-specific antitumor activity of DAT treatment is mainly due to the DAT-induced NF-κB inhibition. Constitutive NF-κB activation is essential for the antiapoptosis and growth of PEL cells (7-9), consistent with our data, the NF-κB inhibitor BAY11-7082, decreased the viability of PEL cells compared to KSHV-uninfected cells (Fig. 4D), and other NF-κB inhibitors also have PEL-specific cytotoxic effects (10,11). In fact, KSHV targets NF-κB signaling to influence gene expression and apoptosis. KSHV-encoded v-FLIP, K15, v-GPCR, K1 and K7 activate NF-κB signaling to achieve antiapoptosis in KSHV-infected cells, including PEL cells (4,6). Therefore, DAT-mediated destabilization of TRAF6 induces stabilization of IκBα and the subsequent inhibition of NF-κB signaling, which in turn may result in apoptosis of PEL cells. NF-κB signaling is also required for KSHV replication (10,11). DAT inhibited virus production at low concentrations, such as 0.2 and 1.0 μM (Fig. 6A), which do not influence proliferation of PEL cells (Fig. 1). DAT administration suppressed the ascites in the peritoneal cavity and the development of KSHV-infected cells in ascites of PEL-xenografted SCID mice (Fig. 7). DAT significantly inhibited the growth and infiltration of PEL cells in vivo and in vitro. Taken together, our data suggest that DAT may serve as a new lead compound for the development of novel drugs against not only PEL but also KSHV infection.

Acknowledgements

References

1. Russo JJ, Bohenzky RA, Chien MC, Chen J, Yan M, Maddalena D, Parry JP, Peruzzi D, Edelman IS, Chang Y, *et al*: Nucleotide sequence of the Kaposi sarcoma-associated herpesvirus (HHV8). Proc Natl Acad Sci USA 93: 14862-14867, 1996.
2. Nador RG, Cesarman E, Chadburn A, Dawson DB, Ansari MQ, Sald J and Knowles DM: Primary effusion lymphoma: A distinct clinicopathologic entity associated with the Kaposi's sarcoma-associated herpes virus. Blood 88: 645-656, 1996.
3. Chang Y, Cesarman E, Pessin MS, Lee F, Culpepper J, Knowles DM and Moore PS: Identification of herpesvirus-like DNA sequences in AIDS-associated Kaposi's sarcoma. Science 266: 1865-1869, 1994.
4. Järviluoma A and Ojala PM: Cell signaling pathways engaged by KSHV. Biochim Biophys Acta 1766: 140-158, 2006.
5. Fujimuro M, Wu FY, ApRhys C, Kajumbula H, Young DB, Hayward GS and Hayward SD: A novel viral mechanism for dysregulation of beta-catenin in Kaposi's sarcoma-associated herpesvirus latency. Nat Med 9: 300-306, 2003.
6. Ashizawa A, Higashi C, Masuda K, Ohga R, Taira T and Fujimuro M: The ubiquitin system and Kaposi's sarcoma-associated herpesvirus. Front Microbiol 3: 66, 2012.
7. Chaudhary PM, Jasmin A, Eby MT and Hood L: Modulation of the NF-κB pathway by virally encoded death effector domains-containing proteins. Oncogene 18: 5738-5746, 1999.
8. Keller SA, Schattner EJ and Cesarman E: Inhibition of NF-kappaB induces apoptosis of KSHV-infected primary effusion lymphoma cells. Blood 96: 2537-2542, 2000.
9. Keller SA, Hernandez-Hopkins D, Vider J, Ponomarev V, Hyjek E, Schattner EJ and Cesarman E: NF-kappaB is essential for the progression of KSHV- and EBV-infected lymphomas in vivo. Blood 107: 3295-3302, 2006.
10. Saji C, Higashi C, Niinaka Y, Yamada K, Noguchi K and Fujimuro M: Proteasome inhibitors induce apoptosis and reduce viral replication in primary effusion lymphoma cells. Biochem Biophys Res Commun 415: 573-578, 2011.
11. Higashi C, Saji C, Yamada K, Kagawa H, Ohga R, Taira T and Fujimuro M: The effects of heat shock protein 90 inhibitors on apoptosis and viral replication in primary effusion lymphoma cells. Biol Pharm Bull 35: 725-730, 2012.
12. Wang G, Gao Y, Li L, Jin G, Cai Z, Chao JI and Lin HK: K63-linked ubiquitination in kinase activation and cancer. Front Oncol 2: 5, 2012.
13. Chen ZJ: Ubiquitination in signaling to and activation of IKK. Immunol Rev 246: 95-106, 2012.
14. Skaug B, Jiang X and Chen ZJ: The role of ubiquitin in NF-kappaB regulatory pathways. Annu Rev Biochem 78: 769-796, 2009.
15. Calvo-Gómez O, Morales-López J and López MG: Solid-phase microextraction-gas chromatographic-mass spectrometric analysis of garlic oil obtained by hydrodistillation. J Chromatogr A 1036: 91-93, 2004.
16. Lawson LD, Wang ZJ and Hughes BG: Identification and HPLC quantitation of the sulfides and dialk(en)yl thiosulfinates in commercial garlic products. Planta Med 57: 363-370, 1991.
17. Yi L and Su Q: Molecular mechanisms for the anti-cancer effects of diallyl disulfide. Food Chem Toxicol 57: 362-370, 2013.
18. Wang HC, Pao J, Lin SY and Sheen LY: Molecular mechanisms of garlic-derived allyl sulfides in the inhibition of skin cancer progression. Ann N Y Acad Sci 1271: 44-52, 2012.
19. You S, Nakanishi E, Kuwata H, Chen J, Nakasone Y, He X, He J, Liu X, Zhang S, Zhang B, *et al*: Inhibitory effects and molecular mechanisms of garlic organosulfur compounds on the production of inflammatory mediators. Mol Nutr Food Res 57: 2049-2060, 2013.
20. Das A, Banik NL and Ray SK: Garlic compounds generate reactive oxygen species leading to activation of stress kinases and cysteine proteases for apoptosis in human glioblastoma T98G and U87MG cells. Cancer 110: 1083-1095, 2007.
21. Chandra-Kuntal K, Lee J and Singh SV: Critical role for reactive oxygen species in apoptosis induction and cell migration inhibition by diallyl trisulfide, a cancer chemopreventive component of garlic. Breast Cancer Res Treat 138: 69-79, 2013.
22. Wang HC, Hsieh SC, Yang JH, Lin SY and Sheen LY: Diallyl trisulfide induces apoptosis of human basal cell carcinoma cells via endoplasmic reticulum stress and the mitochondrial pathway. Nutr Cancer 64: 770-780, 2012.
23. Filomeni G, Rotilio G and Ciriolo MR: Molecular transduction mechanisms of the redox network underlying the antiproliferative effects of allyl compounds from garlic. J Nutr 138: 2053-2057, 2008.
24. Lee HJ, Lee HG, Choi KS, Surh YJ and Na HK: Diallyl trisulfide suppresses dextran sodium sulfate-induced mouse colitis: NF-κB and STAT3 as potential targets. Biochem Biophys Res Commun 437: 267-273, 2013.
25. Shin DY, Kim GY, Hwang HJ, Kim WJ and Choi YH: Diallyl trisulfide-induced apoptosis of bladder cancer cells is caspase-dependent and regulated by PI3K/Akt and JNK pathways. Environ Toxicol Pharmacol 37: 74-83, 2014.
26. Okada S, Goto H and Yotsumoto M: Current status of treatment for primary effusion lymphoma. Intractable Rare Dis Res 3: 65-74, 2014.
27. Wakao K, Watanabe T, Takadama T, Ui S, Shigemi Z, Kagawa H, Higashi C, Ohga R, Taira T and Fujimuro M: Sangivamycin induces apoptosis by suppressing Erk signaling in primary effusion lymphoma cells. Biochem Biophys Res Commun 444: 135-140, 2014.
28. Fujimuro M, Liu J, Zhu J, Yokosawa H and Hayward SD: Regulation of the interaction between glycogen synthase kinase 3 and the Kaposi's sarcoma-associated herpesvirus latency-associated nuclear antigen. J Virol 79: 10429-10441, 2005.
29. Fujimuro M, Sawada H and Yokosawa H: Production and characterization of monoclonal antibodies specific to multi-ubiquitin chains of polyubiquitinated proteins. FEBS Lett 349: 173-180, 1994.
30. Chen C and Okayama H: High-efficiency transformation of mammalian cells by plasmid DNA. Mol Cell Biol 7: 2745-2752, 1987.
31. Milner JA: A historical perspective on garlic and cancer. J Nutr 131 (Suppl 3): 1027S-1031S, 2001.
32. Xiao D, Choi S, Johnson DE, Vogel VG, Johnson CS, Trump DL, Lee YJ and Singh SV: Diallyl trisulfide-induced apoptosis in human prostate cancer cells involves c-Jun N-terminal kinase and extracellular-signal regulated kinase-mediated phosphorylation of Bcl-2. Oncogene 23: 5594-5606, 2004.
33. Antosiewicz J, Herman-Antosiewicz A, Marynowski SW and Singh SV: c-Jun NH(2)-terminal kinase signaling axis regulates diallyl trisulfide-induced generation of reactive oxygen species and cell cycle arrest in human prostate cancer cells. Cancer Res 66: 5379-5386, 2006.
34. Murai M, Inoue T, Suzuki-Karasaki M, Ochiai T, Ra C, Nishida S and Suzuki-Karasaki Y: Diallyl trisulfide sensitizes human melanoma cells to TRAIL-induced cell death by promoting endoplasmic reticulum-mediated apoptosis. Int J Oncol 41: 2029-2037, 2012.
35. Liu KL, Chen HW, Wang RY, Lei YP, Sheen LY and Lii CK: DATS reduces LPS-induced iNOS expression, NO production, oxidative stress, and NF-kappaB activation in RAW 264.7 macrophages. J Agric Food Chem 54: 3472-3478, 2006.
36. Kuo WW, Wang WJ, Tsai CY, Way CL, Hsu HH and Chen LM: Diallyl trisufide (DATS) suppresses high glucose-induced cardiomyocyte apoptosis by inhibiting JNK/NFκB signaling via attenuating ROS generation. Int J Cardiol 168: 270-280, 2013.
37. Wang Z, Xia Q, Cui J, Diao Y and Li J: Reversion of P-glycoprotein-mediated multidrug resistance by diallyl trisulfide in a human osteosarcoma cell line. Oncol Rep 31: 2720-2726, 2014.
38. Nakayama KI and Nakayama K: Ubiquitin ligases: Cell-cycle control and cancer. Nat Rev Cancer 6: 369-381, 2006.
39. Hershko A and Ciechanover A: The ubiquitin system for protein degradation. Annu Rev Biochem 61: 761-807, 1992.
40. Choi YB and Harhaj EW: HTLV-1 tax stabilizes MCL-1 via TRAF6-dependent K63-linked polyubiquitination to promote cell survival and transformation. PLoS Pathog 10: e1004458, 2014.
41. Yang WL, Wang J, Chan CH, Lee SW, Campos AD, Lamothe B, Hur L, Grabiner BC, Lin X, Darnay BG, *et al*: The E3 ligase TRAF6 regulates Akt ubiquitination and activation. Science 325: 1134-1138, 2009.